Eur Radiol (2003) 13:1859–1871
DOI 10.1007/s00330-002-1581-1

Antonios Drevelegas
Danai Chourmouzi
Glikeria Boulogianni
Ioannis Sofroniadis

Imaging of primary bone tumors of the spine

Received: 28 January 2002
Revised: 17 May 2002
Accepted: 14 June 2002
Published online: 25 September 2002

A. Drevelegas · I. Sofroniadis
Ahepa University Hospital,
S. Kyraikidi 1, 54006 Thessaloniki, Greece

D. Chourmouzi (✉) · G. Boulogianni
Asklipios Aristotelio Diagnostic Center,
Papanastasiou 207,
54236 Thessaloniki, Greece
e-mail: dvryz@tee.gr
Fax: +30-31-0327269

Abstract Primary tumors of the spine are relatively infrequent lesions compared with metastatic disease, multiple myeloma, and lymphoma. A wide variety of benign and malignant neoplasms can involve the spine. The imaging features of these lesions are often characteristic. We present an overview of the imaging modalities in primary tumors of the spine in order to provide a useful tool in current radiologic practice. The role of CT and MRI is discussed.

Keywords Spine · Primary neoplasms · CT · MRI

Introduction

Primary tumors of the spine are uncommon, representing less than 5% of all bone neoplasms [1].

In this article we discuss and illustrate the most common benign and malignant primary neoplasms of the spine, including osteoid osteoma, osteoblastoma, osteosarcoma, osteochondroma, chondrosarcoama, malignant fibrous histiocytoma, giant cell tumor, plasmocytoma, Ewing's sarcoma, chordoma, hemangioma, aneurysmal bone cyst, and eosinophilic granuloma (Table 1).

Osteoid osteoma

Osteoid osteoma is a common benign tumor which constitutes 10% of all benign bone tumors. One of the sites of predilection of osteoid osteoma is the vertebral column (13%) [2]. The majority of spinal osteoid osteomas (75%) are located in the posterior elements of the vertebra (pedicles, articular facets, and laminae) and only 7% are in the vertebral body [3].

Most cases of osteoid osteomas present between the ages of 5 and 25 years. The typical patient is a teenager complaining of dull pain, worse at night, which often disappears after administration of salicylates. Scoliosis concave to the side of the tumor is a prominent feature. Osteoid osteoma consists of a well-vascularized nidus of connective tissue, and trabeculae of osteoid and calcified bone surrounded by osteoblasts [2]. Bone scintigraphy demonstrates marked increased uptake by osteoid osteoma nidus. Occasionally, a more distinct double-intensity pattern is apparent with central high degree of radionuclide uptakes surrounded by less intense zone of tracer accumulation corresponding to nidus and osseous reaction [4]. The classic radiographic appearance of osteoid osteoma is a round to oval, discrete radiolucent area (representing the nidus), with variable surrounding sclerosis. On CT, a mineralized center is seen within a well-defined osteolytic lesion surrounded by reactive sclerosis (Fig. 1a). On MR imaging the nidus is low to intermediate signal intensity on T1-weighted images and intermediate to high signal on T2-weighted images. Post-contrast MRI shows enhancement of the lesion. Areas of calcification have low signal intensity on both T1 and T2

Table 1 Primary bone tumors of the spine

Lesion	Patient age	Location in vertebra	Gross histologic features	Imaging features
Osteoid osteoma	Second decade	Posterior elements (75%)	Vascularized connective tissue nidus surrounded by reactive cortical bone	Radio lucent nidus with surrounding sclerosis rarely extended to vertebral body, epidural or paraspinal spaces
		Vertebral body 7% Lumbar 59%, cervical 27% Thoracic 12%, sacral 2%		
Osteoblastoma	Second to third decade	Posterior elements	Osteoid-producing neoplasms	Expansile destructive lesion partially calcified Common extension to vertebral body
		Equally distributed in the cervical, thoracic, and lumbar segments		
Osteosarcoma	Fourth decade	Vertebral body	Osteoid within sarcomatous tissue	Osteosclerotic and osteolytic areas with soft tissue component; common extension to posterior elements
		Lumbosacral region		
Osteochondroma	Third decade	Exclusively to posterior elements Predilection for spinous process Cervical spine	Cartilage cap with normal bone component	Continuity of the lesion with marrow and cortex of the underlying bone
Chondrosarcoma	Fifth decade	Predilection for vertebral body	Hyaline cartilage with increased cellularity within myxoid matrix	Bone destruction with characteristic punctate calcifications
		Thoracic region		
Malignant fibrous histiocytoma	Second to eighth decade	Vertebral body	Mixture of histiocytes, fibroblasts, and primitive mesenchymal cells	Lytic lesion with low signal on T1-weighted and high signal on T2-weighted images
Giant cell tumor	Third decade	Vertebral body Sacrum	Osteoclastic giant cells intermixed with spindle cell	Osteolytic geographic area with soft tissue component
Plasmocytoma	>40 years old	Vertebral body	Sheets of plasma cells on a delicate reticular stroma	Radiolucent areas or reduction in bone density Hypointense on T1-weighted and hyperintense on T2-weighted images
		Thoracic and lumbar spine		
Ewing's sarcoma	10–30 years	Vertebral body Lumbosacral spine	Sheets of round cells	Lytic lesion, associated soft tissue mass
Chordoma	Middle-aged patients	Exclusively affects y vertebral bod Sacrococcygeal 50–60% Sphenooccipital 25–35%	Lobulated mass with mucinous containing cells	Destructive midline expansile lesion with associated soft tissue mass Extension to adjacent vertebra
Hemangiomas	Any age	Vertebral body	Vascular spaces lined by endothelial cells	Vertical parallel densities
	Peak fourth decade	Lower thoracic–upper lumbar regions		Spotted appearance on CT
				High signal on T1-weighted and T2-weighted images Involvement of posterior elements
Aneurysmal bone cyst	Young patients	Posterior osseous elements 60%	Cystic spaces containing blood products	Lytic expansile lesion with fluid–fluid levels
	Less than 20 years	Vertebral body 40%		Involvement of contiguous vertebrae
		Thoracic lumbar		
Langerhans cell histiocytosis	First, second decades	Vertebral body	Sheets of Langerhans cells, lymphocytes, and eosinophils	Lytic lesion of vertebral body leading to collapse
		Rarely posterior elements Thoracic Rarely lumbar, cervical		

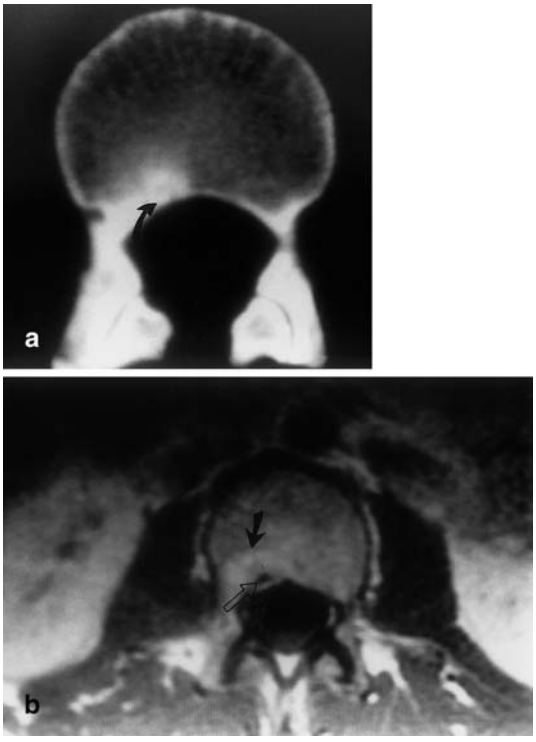

Fig. 1a, b Osteoid osteoma of L3 vertebra. **a** Computed tomography shows a hypodense area surrounded by sclerosis at the posterior cortical surface of the vertebral body. Note the calcified nidus (*arrow*). **b** Axial post-contrast T1-weighted images shows intense enhancement of the lesion (*arrow*) with central low-signal focus corresponding to the calcified nidus (*open arrow*)

images (Fig. 1b). Although soft tissue extension is not a characteristic feature of osteoid osteoma, para-osseous reactive mass may be seen [5]. The histologic differential diagnosis includes osteoblastoma which is a lytic expansile lesion larger than 1.5 cm in diameter, and the radiographic differential diagnosis includes osteomyelitis (Brodie's abscess) which has a history of chronic inflammatory process and enostosis which is an asymptomatic lesion. Standard therapy is surgical removal of the entire nidus.

Osteoblastoma

Osteoblastomas are rare benign primary bone tumors that are histologically similar to osteoid osteoma. These tumors occur in the second and third decades of life. Osteoblastoma most frequently involves the posterior vertebral elements, although extension into the vertebral body is also common. Patients may complain of a dull, localized pain for more than 1 year before diagnosis. Unlike osteoid osteoma, which is confined and self-limited, osteoblastoma may show expansile behavior with epidural and paraspinal spread [4, 6]. Pathologically, osteoblastoma is an osteoid-producing neoplasm that histologically is similar to osteoid osteoma. The typical osteoblastoma is larger than 1.5–2.0 cm in diameter. Plain radiographic findings in osteoblastoma usually demonstrate an expansile destructive lesion that is partially or extensively calcified or ossified and arises from the posterior elements (Fig. 2a). On CT lucent areas of geographic bone destruction corresponding to replacement of bone by nonmineralized tumor osteoid are seen (Fig. 2b). Cloudy, flocculent or ring-like mineralization corresponds to the formation of tumor bone (Fig. 3) [7]. The MR imaging appearance of osteoblastoma is nonspecific, with low to intermediate signal intensity seen on T1-weighted images and intermediate to high signal intensity seen on T2-weighted images (Fig. 2c, d) [8]. The differential diagnosis of osteoblastoma includes osteoid osteoma, which is usually smaller; features more reactive bone and may have a characteristic pain pattern. Aneurysmal bone cyst, which may be larger and more lytic in appearance, giant cell tumor, Ewing's sarcoma, chondrosarcoma, as well as fibrous dysplasia may also be candidates [2].

Osteosarcoma

Osteosarcoma of the spine is rare, accounting for 0.6–3.2% of all osteosarcomas and 5% of all primary malignant tumors of the spine. The peak incidence of spinal osteosarcoma is the fourth decade, it occurs in males more frequently than in females, and has a predilection for the lumbosacral region. The origin of spinal osteosarcoma is the vertebral body, but secondary extension into the posterior elements is also common [9]. Osteosarcoma of the spine may be associated with Paget's disease and previous radiation therapy. One unusual association of osteosarcoma is its presentation as a second tumor approximately 10 years after the detection of retinoblastoma [2, 10]. Patients with spinal osteosarcoma often present with pain and neurologic symptoms. Serum alkaline phosphatase levels may be elevated. On histologic examination, the identification of osteoid formed within and by sarcomatous tissue is essential in establishing the diagnosis [2, 4]. Radiographically, spinal osteosarcoma may be predominantly osteosclerotic but most frequently has mixed osteosclerotic/osteolytic appearance (Fig. 4a). Ivory vertebral body may be recognized, as well as loss of vertebral height, sparing the intervertebral disc [4]. The coexistent soft tissue mass that is a major sign of malignancy and the extent of the lesion can be better appreciated with CT and MRI (Fig. 4b). If osteosarcoma has a prominent sclerotic component, very low signal is seen on both T1 and T2 sequences. After the administration of contrast medium, enhancement of the soft tissue component is seen (Fig. 4c).

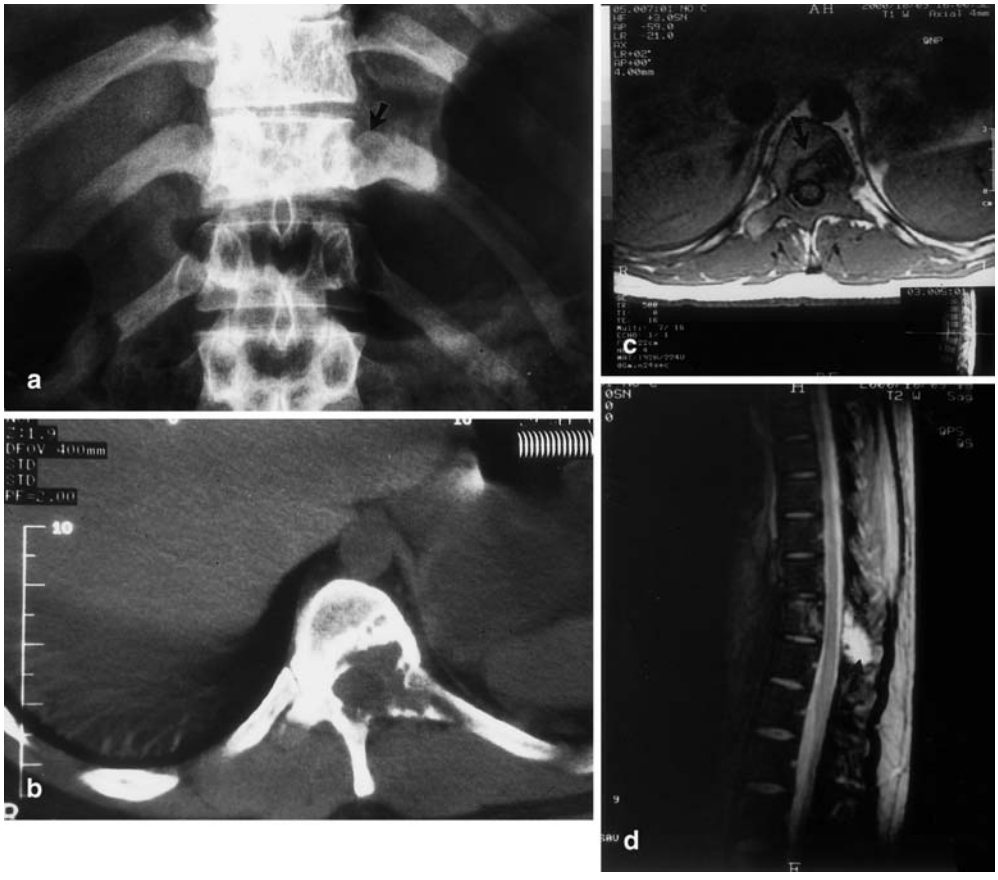

Fig. 2a–d Osteoblastoma of T11 vertebra in a 20-year-old man. **a** Anteroposterior plain film of the thoracic spine shows lytic lesion involving the left side of the vertebral body and the ipsilateral costovertebral joint (*arrow*). **b** On CT the lesion appears with sclerotic margin involving the posterior vertebral body, the left pedicle, as well as the left costovertebral joint. **c** On axial T1-weighted image the lesion shows low and intermediate signal intensity. Note the low-intensity linear area demarcating the lesion from the normal vertebral body (*arrow*). **d** On Sagittal T2-weighted image a high-signal lesion of the T11 vertebral body is seen extending to the posterior elements of the spine (*arrow*)

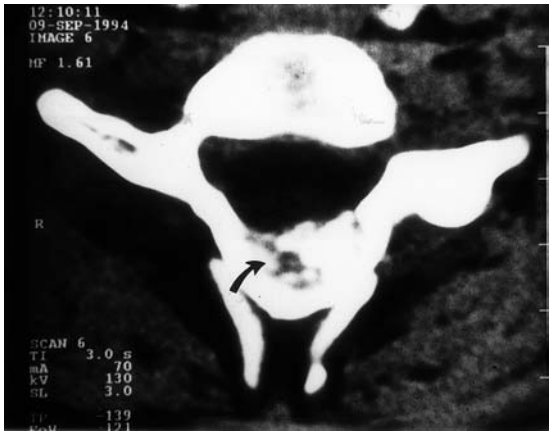

Fig. 3 Osteoblastoma of C6 vertebral in a 15-year-old boy. The CT scan shows a destructive expansile lesion involving the spinous process and laminae with foci of mineralized-osseous matrix (*arrow*)

Osteochondroma

Osteochondromas rarely occur in the spine and have a predilection for the cervical spine [11]. They arise exclusively from posterior elements with predilection for the spinous process [4]. Spinal osteochondromas are usually discovered at the age of 20–30 years in patients with solitary osteochondroma. Rarely, an osteochondroma arises at a site of prior radiation therapy [12]. The most frequent presenting symptom is a palpable mass. When the lesion extends posteriorly myelopathy is not uncommon. Dysphagia and hoarseness may be the presenting symptoms when the lesion is located in the cervical spine and protrudes anteriorly [13]. Pathologically, osteochondromas are composed of two elements, a cartilage cap from which growth occurs and a normal bone component which is attached to the underlying host bone [4, 11]. The pathologic and radiologic hallmark of osteochondroma is continuity of the lesion with the marrow and cortex of the underlying bone. Thin CT sections can detect the marrow and cortical continuity of the lesion to the underlying bone (Fig. 5a). Magnetic resonance imaging reveals the contiguity of yellow marrow with high signal on TI-weighted images and intermediate signal intensity on T2-weighted images centrally and low signal intensity cortex peripherally (Fig. 5b, c).

Chondrosarcoma

The spine represents the primary site in 3–12% of all chondrosarcomas with predilection for the vertebral

Fig. 4a–c Osteosarcoma of the sacrum in a 28-year-old man. **a** Plain film demonstrates a sacral destructive lesion with central osteoid matrix. **b** A CT scan reveals a sacral soft tissue mass with extensive ossified area. **c** Post-contrast axial T1-weighted image shows a peripheral enhanced mass with low-signal central area, which corresponds to the osteoid matrix. Note also the involvement of the right gluteus maximus, piriform, and obturator muscles (*arrow*)

body. Vertebral chondrosarcomas are most common in the thoracic region. The mean age of presentation is 45 years [4]. Clinically, pain and swelling, palpable mass, and neurologic symptoms may indicate the presence of the lesion. Pathologically, chondrosarcoma is composed of hyaline cartilage within myxoid matrix and exhibits increased cellularity, nuclear atypia, and permeation of bony trabeculae. Radiography of spinal chondrosarcoma reveals bone destruction with characteristic punctate, as well as flocculent and ring and arc calcifications, which represent the cartilaginous matrix mineralization. Computed tomography can visualize the integrity of the overlying cortex as well as the distribution, configuration, and extent of calcification within the tumor. The attenuation of the nonmineralized portion of the lesion is often lower than that of muscle, which reflects the relatively high water content of hyaline cartilage [4]. Magnetic resonance nicely demarcates the lobulated contour typical of cartilaginous neoplasm (Fig. 6a). Soft tissue expansion beyond the vertebrae body is delineated by distortion of normal anatomy and by abnormal increased signal on T1-weighted images (Fig. 6b). Areas of mineralization show low signal intensity in both sequences. Involvement of adjacent vertebral levels by extension through the disk is seen in approximately 35% of lesions [14]. The differential diagnosis includes enchondroma, chondromyxoid fibroma, osteosarcoma, and metastasis.

Malignant fibrous histiocytoma

Malignant fibrous histiocytoma (MFH) is a sarcoma that occurs most frequently in soft tissues and rarely in bones. Malignant fibrous histiocytoma occurs from the second through eighth decades of life. The spine is a very uncommon site of localization of this tumor. Histologically, MFH is composed of a mixture of cells resembling fibroblasts, myofibroblasts, histiocytes, and primitive mesenchymal cells. Only sporadic cases have been reported in spine with no documented characteristic findings. Areas of low signal intensity on T1-weighted images and high signal intensity on T2-weighted images are depicted in our case with pathologically proven MFH of C3 vertebra (Fig. 7). Widening of spinal foramina from MFH has been reported in a previous case [15]. The management of malignant fibrous histiocytoma relies on a combination of surgery and chemotherapy.

Giant cell tumor

Giant cell tumors (GCT) of the spine are uncommon lesions that constitute 7% of all cases of GCT. The vast majority of these tumors occur in the sacrum. The GCT shows a predilection for vertebral body rather than the posterior elements. They present between ages of 20 and

Fig. 5a–c Osteochondroma of C7 spinous process. **a** A CT scan of the C7 vertebra shows a posterior exophytic osseous lesion protruding into the spinal canal. **b**, **c** T1- and T2-weighted sagittal images demonstrate the signal intensity characteristic of yellow marrow within the osteochondroma causing impingement on the spinal cord (*arrows*)

40 years and are rarely encountered before the closure of the epiphyseal plate. Dramatic increase in size can be associated with pregnancy and is presumably related to hormonal stimulation [4, 16]. Aneurysmal bone cysts arising in a pre-existing GCT is not an uncommon entity. Pain and neurologic deficits are the most common presenting symptoms. Pathologically, GCTs are composed of osteoclastic giant cells intermixed with spindle cell stroma [17]. Cystic areas as well as areas of previous hemorrhage with hemosiderin are also seen. In addition, areas of fibrous tissue that are high in collagen content are a frequent finding. The radiographic appearance of GCT includes a large lytic geographic area without host response of the underlying bone. In the spine the destruction of the vertebral body is more frequent than that of the posterior osseous elements. Sacral lesions are osteolytic and, owing to their large size and soft tissue component, may simulate the appearance of a malignant neoplasm. On CT the tumor has soft tissue density with well-defined margins. Areas of hemorrhage or necrosis may create foci of low attenuation. No areas of mineralized matrix are seen (Fig. 8). On MR images the lesion shows heterogeneous signal intensity. Generally, the tumor has low to intermediate signal intensity on both T1- and T2-weighted sequences due to the presence of collagen and hemosiderin within it [18]. Evidence of hemorrhage (with high signal intensity on both T1 and T2 images) as well as focal cystic areas (with low signal intensity on T1 and high signal intensity on T2 images) may also be seen. A low signal intensity pseudocapsule is also a common imaging finding [4].

Other sacral lesions that can mimic GCTs include metastatic disease, plasmacytoma, chordoma, "brown tumor" in hyperparathyroidism, and malignant nerve sheath tumors.

Multiple myeloma–plasmacytoma

Multiple myeloma (MM) is a monoclonal proliferation of malignant plasma cells of bone marrow. The vertebrae are affected in 66% of the patients [19]. The thoracic and

Fig. 6a, b Chondrosarcoma of the cervical spine. **a** Sagittal T2-weighted image reveals a large lobulated soft tissue mass with high signal intensity involving the C2 vertebrae. **b** Axial T1-weighted image shows an intermediate signal intensity mass originating from the C2 vertebral body with upper airway tract compression

lumbar regions are most commonly involved. Persons over the age of 40 years are most commonly affected. Plasmacytoma refers to the solitary form of the disease and is usually found in younger patients more than MM. Patients present with bone pain, fatigue, anemia, and neurologic symptoms secondary to compression of the spinal cord. On histologic examination sheets of plasma cells on a delicate reticular stroma characterize myeloma. Two classic radiographic features are encountered on plain radiographs: generalized reduction in bone density with thickening trabeculae and localized radiolucent areas without reactive marginal sclerosis involving the vertebral body. The ivory vertebral pattern has also been reported. On MR images, the characteristics of plasmacytomas are nonspecific: hypointense to healthy marrow on T1-weighted images and hyperintense on T2-weighted images [19, 20]. As the disease advances, multiple foci destruction, almost invariably accompanied by some degree of collapse of the affected vertebral bodies, is likely to be present. Aggressive cortical disruption and infiltration into soft tissue and adjacent structures can be identified on MR examination. An involved vertebral body may collapse and disappear completely. Differentiation from inflammatory lesions can be made, as the intervertebral disc spaces and the articular surfaces are not affected (Fig. 9).

Ewing's sarcoma

Ewing's sarcoma is one of the malignant round-cell tumors involving the bones. The spine is the site of origin in 4–18% of Ewing's sarcomas [21]. The lumbosacral spine is the most common site. Lesions typically occur in the vertebral bodies. Most lesions occur between 10 and 30 years of age.

Nonspecific nature of pain is the most common presenting symptom. Histologically, Ewing's sarcoma is composed of sheets of small, closely spaced cells with scant cytoplasm and a single oval or round nucleus. The classic radiologic presentation is that of a lytic tumor which is often permeative. Lesions are usually lytic but may be mixed with areas of sclerosis. Occasionally, Ewing's sarcoma is predominately sclerotic. Complete collapse of vertebral body may be seen. Computed tomography shows the pattern of bone destruction and associated soft tissue mass which is a prominent feature of Ewing's sarcoma. The MR imaging appearance is nonspecific with lesions showing low to intermediate signal intensity on T1-weighed images and intermediate to high signal intensity on T2-weighted images. The differential diagnosis of Ewing's sarcoma includes pyogenic or tuberculous osteomyelitis, lymphoma, leukemia, histiocytosis and metastatic disease.

Chordoma

Chordoma is a low-grade malignant tumor. These tumors arise from the remnants of embryonic notochord. They accounts for approximately 2–4% of the malignant neoplasms of the bone. The most common site of tumor development include the sacrococcygeal region (50–60%), sphenooccipital region (25–35%), and spine (15%). In the spine this tumor exclusively affects the vertebral body with common extension through the disk to involve the adjacent vertebra. Chordoma occurs most commonly in middle-aged patients (aged 30–60 years) Symptoms relate to the site of the lesion as well as the degree of the extension. Gradual-onset radicular pain and sensory problems are the primary neurologic symptoms. Dysphagia as a predominant symptom on initial presentation of cervical chordoma, although rare, has been reported in

Fig. 7a, b Malignant fibrous histiocytoma. **a** T1-weighted sagittal image shows low signal intensity of the C3 vertebral body with enlargement of its anteroposterior diameter (*arrow*). **b** T2-weighted sagittal image shows focal areas of high signal within the C3 vertebral body

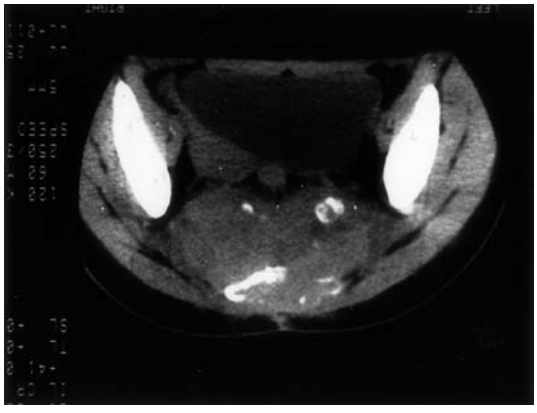

Fig. 8 Giant cell tumor of the sacrum. The CT scan shows a destructive lesion of the sacrum with large soft tissue component

Fig. 9a, b Plasmatocytoma. **a** Sagittal T2-weighted and **b** sagittal post-contrast T1-weighted image show a severely collapsed T12 vertebra with low signal intensity and large soft tissue mass filling the spinal canal. Note the preservation of the adjacent intervertebral disks

the literature [22]. Incontinence or constipation may be clinical presentations in sacral lesions. On gross inspection the classic chordoma is a lobulated mass contained within a pseudocapsule. Microscopically, fibrous strands create characteristic lobules of either predominantly mucin-containing physaliphorous (bubble-like) cells or frankly cystic mucinous pool [23]. The most frequent radiographic appearance is that of a destructive expansile lesion of vertebral body centered in the midline with a large associated soft tissue mass. There may be intervertebral disk involvement. Similarly, sacrococcygeal chordomas may extend across the sacroiliac joint [4].

Images on CT reveal destruction of bone without any associated sclerosis and low attenuation within the soft tissue mass, which is due to gelatinous material and cystic degeneration within the tumor. Intratumoral calcifications that represent sequestra of destroyed bone rather than tumoral calcification are seen in 90% of sacrococcygeal lesions on CT scans (see Fig. 11a) [24]. Spinal chordoma mimics neurofibroma when enlargement of the intervertebral foramen by the tumor occurs (Fig. 10). Contrast enhancement on CT is usually mild to moderate and is heterogeneous. Chordomas on MR images have low to intermediate signal intensity on T1-weighted images, although they may have areas of high signal intensity related to high protein content or hemorrhage

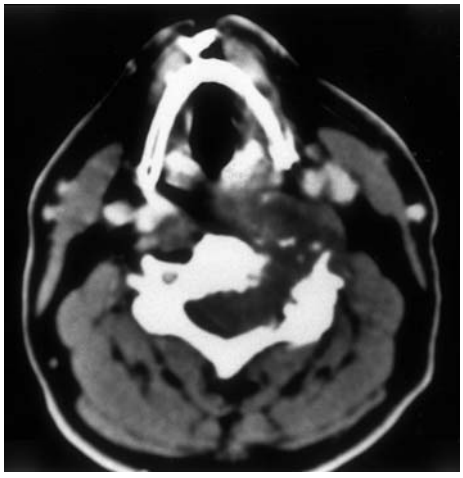

Fig. 10 Chordoma of C3 vertebra. The CT shows a soft tissue mass causing enlargement of the left intervertebral foramen. Note the internal foci of calcification and the extension of the mass anteriorly

(Fig. 11b). They have very high signal intensity on T2-weighted images similar to the nucleus polposus [4]. Fibrous septae of low-signal intensity within the tumor have been reported on T2-weighted images in 70% of chordomas (Fig. 11c) [25]. Although CT and MR imaging vary, chordoma should be considered when a destructive lesion of vertebral body is associated with a large well-defined mass that is hyperintense on T2-weighted images (Fig. 12). Spinal chordomas produce radiographic findings that are also evident in skeletal metastasis, plasma cell myeloma, lymphoma, chondrosarcoma, giant cell tumor, and infection.

Hemangiomas

Approximately half of solitary hemangiomas of bone occur in vertebrae. They present at any age with peak incidence the fifth decade of life. Within the spine, hemangiomas are most commonly situated in the lower thoracic and upper lumbar regions. The vertebral body is the most common location; however, hemangioma rarely extends beyond the vertebral body to involve the posterior elements. Hemangioma of bone is by definition a benign lesion composed of vascular spaces lined by endothelial cells. Vertebral hemangiomas are usually small and asymptomatic, although they become symptomatic, with pain being the most common clinical presentation due to compression fracture. Minimal trauma in large lesions leads to pathologic fractures. When hemangiomas reach a considerable size, they extend beyond the confines of the bony margins of the vertebral body. Pregnancy-related vertebral hemangioma compressive myelopathy is a rare occurrence that tends to arise in the upper thoracic

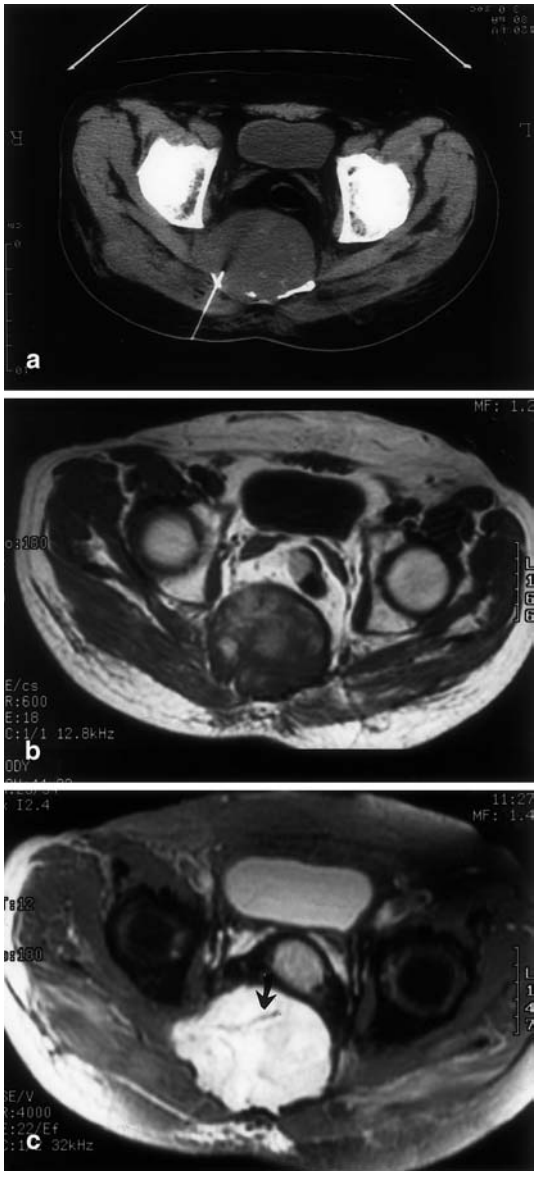

Fig. 11 Chordoma of the sacrum. **a** The CT scan shows a large destructive lesion of the sacrum with soft tissue density and internal foci of calcifications. Note the needle of biopsy which establishes the diagnosis. **b** Axial T1-weighted image shows a well-marginated sacrococcygeal lesion with interspersed high-signal areas. **c** Axial T2-weighted image shows high signal intensity mass with internal low signal septae (*arrow*)

and lower cervical spine, peaks during the third trimester, and remits after parturition. Hemodynamic changes during pregnancy lead to spinal cord compression due to tumor expansion [26]. The classic radiographic appearance of hemangioma includes diminished vertebral density and coarse vertical striation of the vertebral body. In some cases, a honeycomb appearance may be present. These patterns are the result of replacement of bony trabeculae by vascular channels within the vertebrae and

Fig. 12a, b Chordoma of L3 vertebra. **a** Sagittal T2-weighted and **b** axial T1-weighted images show an expansile lesion of the L3 vertebral body with high-signal intensity on T2 and intermediate signal intensity on T1 extending into the spinal canal and compressing the dural sac

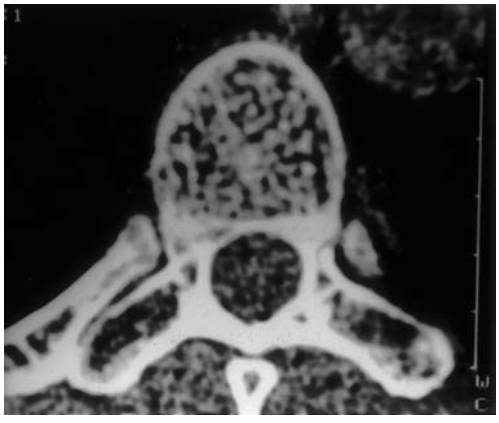

Fig. 13 Axial CT section demonstrates the "polka dot" appearance of the vertebral body, which is pathognomonic for hemangioma

Fig. 14a, b Hemangioma of T6 vertebrae. Sagittal T1- and T2-weighted images of the thoracic spine shows wedge-shaped appearance of the T6 vertebral body with low signal intensity on **a** T1-weighted image and diffuse high signal intensity on **b** T2-weighted image due to bone marrow edema

thickening of the remaining trabeculae [16]. On CT images the classic "polka dot" appearance is pathognomonic for hemangioma. The dots on CT, which represent the thickened trabeculae, correlate with the striated appearance seen on plain radiographs (Fig. 13). Hemangiomas exhibit homogeneous high signal intensity on both T1- and T2-weighted MR images as a result of an increased amount of fat within it. After the administration of paramagnetic agent, they enhance strongly [27]; however, these signal characteristics, while present in asymptomatic patients, may not be present in those patients in whom the hemangioma has led to vertebral compression. In such cases T1-weighted images may show decreased signal within the vertebral body (Fig. 14). The extraosseous matrix of large, complicated hemangiomas displays low (soft tissue) signal intensity on T1-weighted images also (Fig. 15). Focal fat deposition within the spine may mimic vertebral hemangiomas on T1-weighted images, but fail to have the same increased signal intensity on T2-weighted studies.

Langerhans cell histiocytosis

Eosinophilic granuloma (EG) of the bone is the localized and the most benign form of Langerhans cell histiocytosis (LCH). The vertebrae are the primary location of the lesion in 20% of cases. Children, especially boys, between 3 and 12 years are the most commonly affected

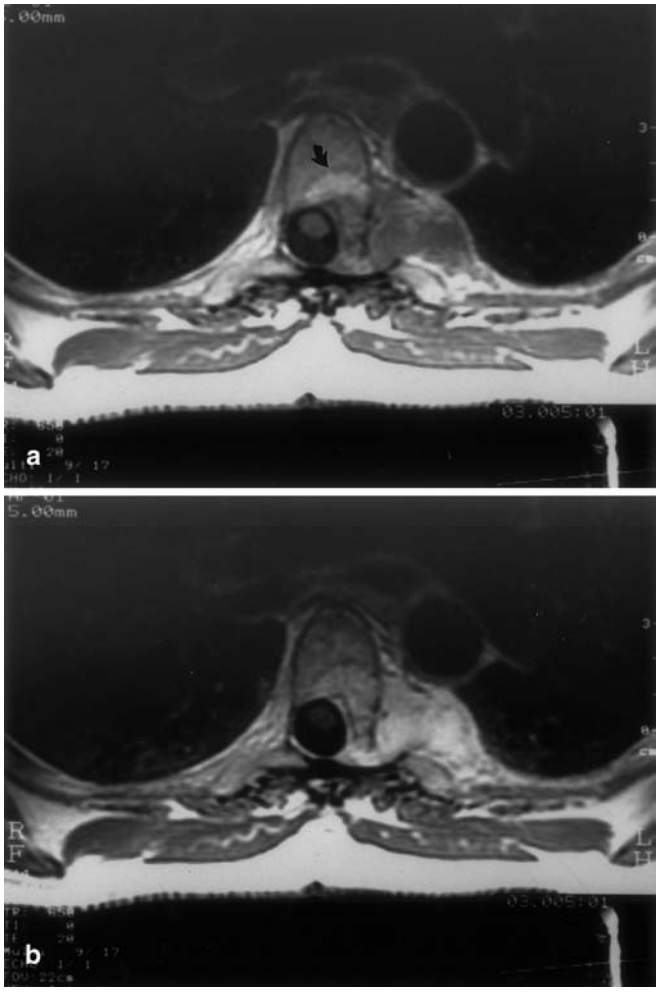

Fig. 15a, b Vertebral hemangioma with paraspinal soft tissue mass. **a** Axial T1-weighted image shows the characteristic high signal intensity of hemangioma in the posterior part of the thoracic vertebra (*arrow*). Note also the paraspinal mass with intraspinal–extradural extension. **b** Axial T1-weighted image after the administration of paramagnetic agent shows intense homogeneous enhancement of the posterior part of the vertebral body as well as of the paraspinal mass

Fig. 16 Langerhans cells histiocytosis in a 35-year-old man. Sagittal T1-weighted image of the thoracic spine shows multiple low-signal lesions in the vertebral bodies. The T8 vertebra is almost completely collapsed

[28]. Pathologically, lesions characteristically consist of sheets of Langerhans cells with variable numbers of lymphocytes, polymorphonuclear cells, and eosinophils in the spine and the vertebral body usually are involved. Isolated involvement of the posterior elements is rare. The thoracic spine is the most common site of the disease. Clinically, the lesion is characterized by local pain, although lesions may also be silent. Low-grade fever, elevated erythrocyte sedimentation rate, mild leukocytosis, and normochronic anemia are findings usually seen. Symptoms of spinal cord compression by eosinophilic granuloma are reported [29]. Eosinophilic granuloma is a rapidly growing lytic lesion of the vertebral body leading to progressive collapse (vertebra plana) with preservation of the adjacent disc space. An associated paraspinal mass may represent soft tissue edema and hemorrhage related to the vertebral collapse or soft tissue extension of LCH. The classical radiographic picture of vertebra plana is easily made from plain radiograph. Computed tomography and MR imaging are useful in outlining the extension of the disease. Lesions are usually lytic on CT with no specific MR signal characteristics. Areas of marrow replacement with low signal intensity on T1-weighted images and high signal on T2 are usually seen (Fig. 16). With healing, there is reconstruction of the involved vertebrae toward the original height, although some residual compression deformity usually persists. The differential diagnosis of collapse of a single vertebral body includes Ewing's sarcoma, metastatic neuroblastoma, idiopathic osteonecrosis, or atypical tuberculus spondylitis. The EG is often a self-limited condition characterized by regeneration of vertebral body. Treatment is controversial and ranges from immobilization, curettage, and intratumoral injection of steroids, to radiation therapy and surgical excision.

Aneurysmal bone cyst

Aneurysmal bone cyst (ABC) is a benign, highly vascular bony lesion. The vertebral column is involved in

3–20% of cases. Most of them occur within the first 2 decades of life The thoracic spine is affected most commonly [30]. Vertebral aneurysmal bone cysts generally arise in the posterior osseous elements. Involvement of contiguous vertebrae may occur. Between 30 and 50% of ABC's are believed to arise within some other preexisting lesions (GCT, chondrosarcoma, chondromyxoid fibroma, nonossifying fibroma, osteoblastoma) [2]. The presenting symptoms include pain and neurologic deficits resulting from encroachment on the spinal canal. Pathologically, ABC has a characteristic honeycomb appearance with various-sized cystic spaces containing both fresh and old blood products [31]. Computed tomography of spinal ABC shows lytic expansile lesion centered in the posterior elements alone or in combination with vertebral body. Expansion is usually most prominent with involvement of the adjacent vertebrae and extension into neighboring rib (Fig. 17). Significant extension into adjacent soft tissues also may occur [4, 16]. Both CT and MR clearly show the cystic nature of the lesion with single or multiple fluid–fluid levels indicative of hemorrhage with sedimentation. Although highly suggestive of ABC, fluid–fluid levels are nonspecific, having been reported in benign and malignant entities. The MR images are more sensitive in detection of areas with fluid–fluid levels. On T1- or T2-weighted images, they may have increased signal intensity due to methemoglobin in either the dependent or nondependent component (Fig. 18).

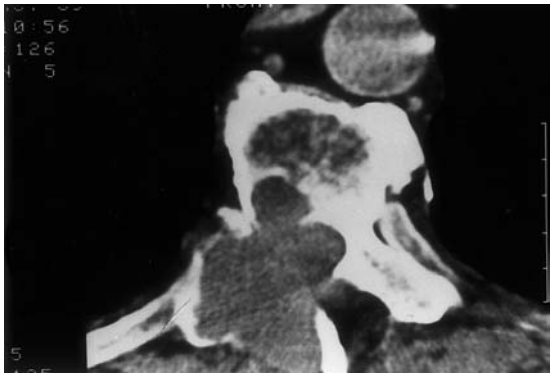

Fig. 17 Aneurysmal bone cyst of thoracic vertebra. The CT scan shows a cystic lesion with scalloped sclerotic margins involving the posterior elements, the vertebral body, as well as the costovertebral joint

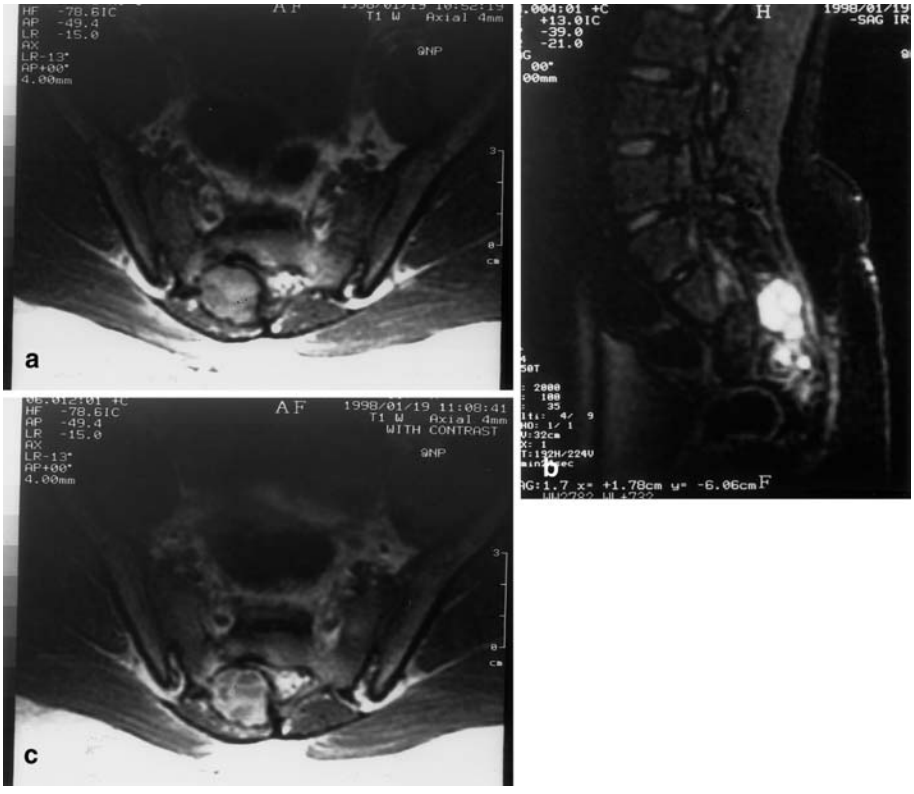

Fig. 18a–c Aneurysmal cyst of the sacrum. **a** Axial T1-weighted image shows a lobulated multiseptated high-signal lesion of the sacrum compressing the neural roots. The high signal intensity is due to the hemorrhagic content of the lesion. **b** On sagittal T2-weighted image the lesion appears multilocular with high signal intensity. **c** After administration of paramagnetic contrast agent, enhancement of internal septae is seen. The fluid–fluid level appearance of the lesion is better depicted

References

1. Masaryk TJ (1991) Neoplastic disease of the spine. Radiol Clin North Am 29: 829–845
2. Bloem JL, Kroon HM (1993) Osseous lesions. Radiol Clin North Am 31:261–278
3. Greenspan A (1993) Benign bone-forming lesions: osteoma, osteoid osteoma, and osteoblastoma. Clinical, imaging, pathologic, and differential consideration. Skeletal Radiol 22:485–500
4. Murphey MD, Andrews CL, Flemming DJ, Temple HT, Smith WS, Smirniotopoulos (1996) Primary tumors of the spine: radiologic–pathologic correlation. Radiographics 16:1131–1158
5. Woods ER, Martel W, Mandell SH, Crabbe JP (1993) Reactive soft tissue mass associated with osteoid osteoma: correlation of MR imaging features with pathologic findings. Radiology 186:221–225
6. Paige ML, Michael AS, Brodin A (1991) Case report 647: benign osteoblastoma causing spinal cord compression and spastic paresis. Skeletal Radiol 20:54–57
7. Ozkal E, Erongun U, Cakir B et al. (1996) CT and MR imaging of vertebral osteoblastoma. A report of two cases. Clin Imaging 20:37–41
8. Kroon HM, Schurmans J (1990) Osteoblastoma: clinical and radiologic findings in 98 new cases. Radiology 175:783–790
9. Wiight NB, Skinner R, Lee RE, Craft AW (1995) Osteogenic sarcoma of the neural arch. Pediatr Radiol 25:62–63
10. Enzmann DR, Paz RL de la (1990) Bone tumors. In: Enzmann DR, Paz RL de la, Rubin JB (eds) Magnetic resonance of the spine. Mosby, St. Louis, pp 413–420
11. Giudici MA, Moser RP Jr, Kransdorf MJ (1993) Cartilaginous bone tumors [review]. Radiol Clin North Am 31:237–259
12. Cree AK, Hadlow AT, Taylor TK, Chapman GK (1994) Radiation-induced osteochondroma in lumbar spine. Spine 19:376–379
13. Barros FTE, Oliveria RP, Taricco MA, Gonzalez CH (1995) Hereditary multiple exostoses and cervical ventral protuberance causing dysphagia. A case report. Spine 20:1640–1642
14. Hermann G, Sacher M, Lanzieri CF, Anderson PJ, Rabinowitz JG (1985) Chondrosarcoma of spine: an unusual radiographic presentation. Skeletal Radiol 14:178–183
15. Zibis AH, Marconis A, Karantanas AH (2000) Unusual cases of spinal foraminal widening. Eur Radiol 10:144–148
16. Conway WF, Hayes CW (1993) Miscellaneous lesions of bone [review]. Radiol Clin North Am 31:339–358
17. Resnick D (1995) Tumors and tumor-like diseases. In: Diagnosis of bone and joint disorders, 3rd edn. Saunders, Philadelphia, pp 3785–3806
18. Murphey MD, Smith WS, Al-Assir, Shekitka KM (1995) MR imaging of giant cell tumor of bone: signal intensity characteristics with radiologic–pathologic correlation. Radiology 197:195
19. Bazan C (1993) Imaging of lumbosacral spine neoplasms. Neuroimaging Clin North Am 3:591–608
20. Liauger J, Palmer J, Amores S, Bague S, Camins A (2000) Primary tumors of the sacrum. Am J Roentgenol 174:417–424
21. Eggli KD, Quigue T, Moser RP (1993) Ewing sarcoma. Radiol Clin North Am 31:325–337
22. Hester TO, Valentino J, Strottmann JM, Blades DA, Robinson M C (1999) Cervicothoracic chordoma presenting as progressive dyspnea and dysphagia. Otolaryngol Head Neck Surg 120:97–100
23. Wippold F, Koeller KK, Smirniotopoulos JG (1999) Clinical and imaging features of cervical chordoma. Am J Roentgenol 172:1423–1426
24. De Bruine FT, Kroon HM (1988) Spinal chordoma: radiologic features in 14 cases. Am J Roentgenol 150:861–863
25. Murphy JM, Wallis F, Toland J, Toner M, Wilson GF (1998) CT and MRI appearances of a thoracic chordoma. Eur Radiol 8:1677–1679
26. Schwartz TH, Hibshoosh H, Riedel CJ (2000) Estrogen and progesterone receptor-negative T11 vertebral hemangioma presenting as a postpartum compression fracture: case report and management. Neurosurgery 46:218–221
27. Ross JS, Masaryk TJ, Modic MT et al. (1987) Vertebral hemangiomas: MR imaging. Radiology 165:165
28. Stull MA, Kransdorf MJ, Devaney KO (1992) Langerhans cell histiocytosis of bone. Radiographics 12:801–823
29. Duarte-Silva EB, Noujaim J el-K, Carnevale F (1999) Cervical spine cord compression by eosinophilic granuloma. Case report. Arq Neuropsiquiatr 57:498–503
30. Koci TM, Mehringer CM, Yamagata N, Chiang F (1995) Aneurysmal bone cyst of the thoracic spine: evolution after particula embolization. Am J Neuroradiol 16:857–860
31. Kransdorf MJ, Sweet DE (1995) Aneurysmal bone cyst: concept, controversy, clinical presentation, and imaging. Am J Roentgenol 164:573–580